IEEE Access
Multidisciplinary ⋮ Rapid Review ⋮ Open Access Journal

Received February 26, 2022, accepted March 11, 2022, date of publication March 21, 2022, date of current version March 28, 2022.

Digital Object Identifier 10.1109/ACCESS.2022.3160724

Dual-Band (28/38 GHz) Wideband MIMO Antenna for 5G Mobile Applications

ASMAA E. FARAHAT AND KHALID F. A. HUSSEIN
Microwave Engineering Department, Electronics Research Institute, Cairo 11843, Egypt
Corresponding author: Asmaa E. Farahat (asmaa@eri.sci.eg)

ABSTRACT A dual-band wideband composite patch antenna constructed from a modified circular primary patch and secondary parasitic patch element is presented in this work. A microstrip feed line is employed to inset-feed the primary patch. The secondary patch is fed indirectly through edge coupling with the main patch. The composite antenna is printed on Rogers Ro3003^{TM} with $\epsilon_r = 3$ and thickness 0.25 mm. The antenna design stages are presented in detail. A MIMO antenna system is constructed from two elements of the proposed composite patch with two different configurations. A prototype is fabricated for the single element and the two-port MIMO antenna configurations. Numerical and experimental results are presented showing good performance regarding impedance matching at the operating bands 28 and 38 GHz, bandwidth, radiation patterns, and gain. The impedance matching bandwidths are 1.23 GHz at 28 GHz and about 1.06 GHz at 38 GHz. The minimum value of the reflection coefficient for 28 GHz 28 GHz band is -34.5 and is -27.3 dB for 38 GHz. The gain of the radiation pattern has a peak of 6.6 dBi at 28 GHz and 5.86 dBi at 38 GHz. For both bands, the radiation patterns are balloon-like omnidirectional. The antenna total dimensions are $7.5 \times 8.8 \times 0.25$ excluding the transmission line. The MIMO system with two-ports for both proposed configurations has appropriate values for ECC and the DG which are calculated through electromagnetic simulations.

INDEX TERMS Fifth generation, MIMO, printed patch.

I. INTRODUCTION

During the last decade, progress in wireless mobile communications with higher bandwidths and data rates is reported. The hunger for endless users joining the network with high rates of information being sent and received has been the driving force behind the boom of the auspicious Fifth-Generation (5G) technology. The data rates have massively exploded to reach 100 times nowadays and as expected, 1000 times by 2030 [1]. The 30-300 GHz Millimeter-wave spectrum is anticipated to be dominant because of its high rate of data transmission to fulfill the needs of the proliferation of 5G applications [2]–[5]. The frequency bands of interest for the fifth generation are 28 GHz, 38 GHz, 60 GHz, and 73 GHz [6].The Federal Communications Commission (FCC) has allocated unlicensed bands in the range 59-64 GHz for high speed communications and short range communication [7]. The International Telecommunications Union (ITU) has allocated certain bands for mobile communication in the fifth generation at 28, 38, 60, and 73 GHz [8].

Antenna design in the mm-wave range poses a set of challenges to the antenna community. Bandwidth augmentation and size reduction are dominant design attentions for the applied utilization of printed antennas. For new RF designs the antenna elements should have low profile, dual or multiple bands of operations, low cost, modest planar design, and squeezed size [9]. Mobile phones are restricted by a very limited space which necessitates the designers to reduce the antenna size with good performance.

Recently, a lot of antennas designed to be employed in mobile phones for fifth generation are provided. Several planar mm-wave antennas with single band are reported in [10]–[13]. Printed mm-wave antennas with dual-band are reported in [14]–[16]. In [14] the designed dual-band antenna achieves a bandwidth of 3% at 28 GHz and 1.9% at 38 GHz. A reconfigurable dual band antenna with ideal switching concept is introduced in [15] but it was not suitable for practical implementation. In [16], narrow bandwidth dual-band antenna at 37.5/47.8 GHz is proposed. In the work of [17],

The associate editor coordinating the review of this manuscript and approving it for publication was Shah Nawaz Burokur.

a tri-band mm-wave antenna at 28/38/48 GHz is presented to be used in the base stations. In the work of [18], four-band MIMO antenna system operating at 28, 43, 52, and 57 GHz is proposed.

The composite microstrip patch antenna proposed in this work uses the 28/38 GHz mm-wave bands in a single antenna with compact size and light weight for the fifth generation mobile handsets. The proposed single-element patch is used to construct a two-port MIMO antenna system. The proposed antenna can also be used to construct compact antenna arrays to be used in beam forming and direction of arrival detection as the adjacent elements have very weak coupling coefficients. The designed composite antenna is fabricated for experimental validation of the simulation results.

II. THE PROPOSED DUAL-BAND MICROSTRIP PATCH DESIGN

The composite patch antenna structure with dual-band operation proposed in this work is shown in Fig. 1. It is constructed from two patches; the primary patch is fed through a direct microstrip line with an inset feed, while the secondary one is edge coupled to the primary patch which acts as indirect feeder to it. First, a primary circular patch is designed to resonate at 28 GHz. The patch is then modified by removing the parts with insignificant current density then its dimensions are modified so that it still resonates at 28 GHz. A secondary parasitic patch is capacitively coupled to the primary patch to match the impedance at another resonance 38 GHz. The secondary patch dimensions are selected such that the two patches together have another resonance at 38 GHz. At the first resonance at 28 GHz, the radiated field pattern is produced mainly due to the primary patch. The radiation pattern is omnidirectional and directed to the upper half-space. At 38 GHz, the two patches contribute to the radiation pattern through the first and the higher order modes which results in undesired side lobes and nulls in the radiation pattern. The cuts made in the primary patch along with the addition of the secondary parasitic patch have the role of modifying the current distributions on the patch surface and the electric fields within the slots, thereby, enhance the first order mode radiation and diminish the higher order mode radiations. The geometry of the composite patch antenna designed in this work is illustrated in Fig. 1 with the dimensional parameters shown on the figure. The substrate used in the design is Ro3003 with $\varepsilon_r = 3.0$ and height 0.25 mm and loss tangent 0.001. The final dimensions of the printed antenna structure are 7.5mm $\times$ 8.8mm $\times$ 0.25 mm. A defect is made in the ground as shown in Fig.1 as dotted red line to increase the antenna bandwidth. The dimensional parameters of the design are listed in Table 1.

III. MIMO ANTENNA SYSTEM CONFIGURATIONS

The proposed composite patch antenna is used to construct a MIMO system for mobile handset for the fifth generation. The MIMO is constructed of two elements placed either side-by-side or front-to-front as shown in Fig. 2a and 2b,

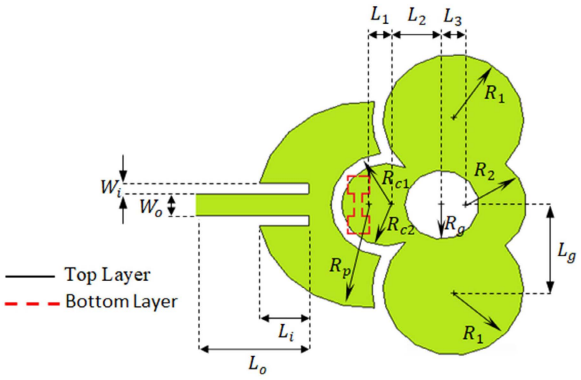

FIGURE 1. Composite geometry of the proposed patch antenna with the dimensional parameters.

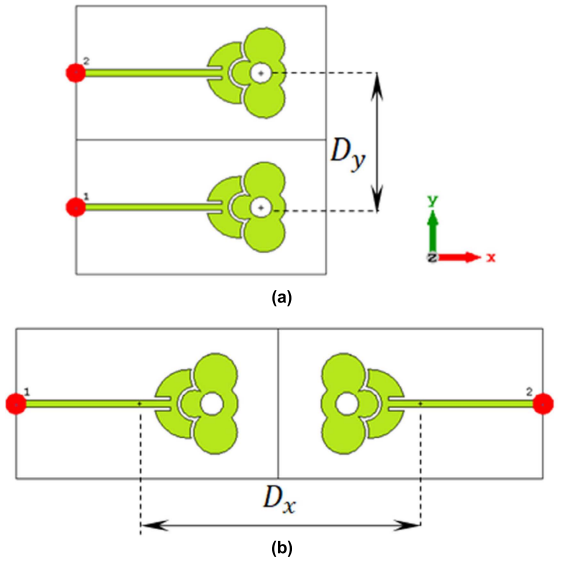

FIGURE 2. MIMO antenna System Configurations (a) side-by-side, (b) front-to-front.

respectively. The two configurations allow for good spatial diversity with high performance due to low mutual coupling coefficients. The two MIMO systems performance are studied regarding the envelope correlation coefficient and the diversity gain over the two operating bands 28 and 38 GHz.

IV. RESULTS AND DISCUSSIONS

The performance of the designed dual-band patch antenna is investigated in this section. The development stages of the proposed microstrip patch design process are illustrated. The numerical results using electromagnetic simulation and experimental measurements for the single element reflection coefficient and the radiation pattern is presented and discussed.

A. DEVELOPMENT STAGES OF THE DUAL-BAND PATCH ANTENNA DESIGN

In this section the design stages of the proposed antenna is demonstrated showing the steps for designing the primary and secondary patches to achieve the dual band operation of the composite antenna structure.

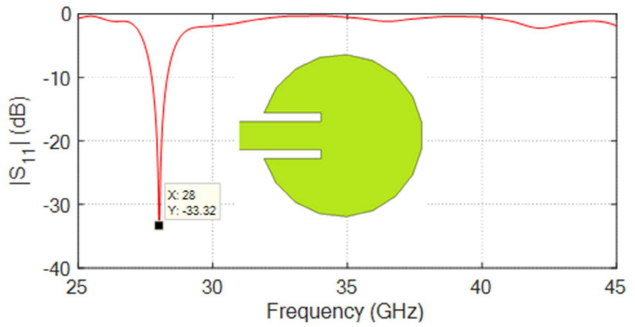

FIGURE 3. The return loss, $|S_{11}|$ for circular patch antenna with inset feed designed to operate at 28 GHz.

1) DESIGN STAGE 1: CIRCULAR PATCH ANTENNA WITH INSET FEED

Preliminarily, a circular patch antenna as that shown in Fig. 3 is designed to resonate at 28 GHz. The frequency dependence of the reflection coefficient $|S_{11}|$, is shown in Fig. 3. As the patch antenna is matched to 50Ω feeding line at 28 GHz, a surface current of significant magnitude is distributed over a wide area of the patch as can be seen in Fig. 4a. The corresponding gain pattern at 28 GHz has an appropriate (balloon-like) shape as shown in Fig. 4b showing maximum gain of about 8 dB in the forward direction ($\theta = 0°$). The current distribution and the gain pattern at 38 GHz are presented in Fig. 5a and 5b, respectively. As the antenna impedance has not yet been matched at 38 GHz, the surface current distribution is concentrated in a very narrow area at the feed position as presented in Fig. 5a when compared to the current distribution at 28 GHz shown in Fig. 4a. Consequently, the gain pattern resulting at 38 GHz shows a wide beam with very low gain of about -2.2 dBi in the forward direction ($\theta = 0°$). The areas on the patch with significant current magnitude are designated as the active region and this region contribute to the radiation in the far zone. By comparison between Fig. 4a and 5a, it can be shown that the active region of the patch at 28 GHz is much wider than the active region at 38 GHz. This results in wider beam radiation pattern at 38 GHz than at 28 GHz as shown in Fig. 4b and 5b. The radiation pattern obtained at 38 GHz is not appropriate for most of the intended applications in 5G mobile handsets due to the wide beam and low gain in the forward direction $\theta = 0°$.

2) DESIGN STAGE 2: MODIFYING THE GEOMETRY OF THE CIRCULAR PATCH

In order to get the antenna matched at 38 GHz, and to improve the corresponding radiation pattern, the geometry of the circular patch described in section A. A.1. is modified as shown in Fig. 6. The geometry modification should keep the impedance matching at 28 GHz. In consequence, the idea behind the suggested geometrical modification is to reduce the patch area so as to get another resonance at the higher frequency (38 GHz) by removing the part of the patch that carries relatively weak current at the first resonance (28 GHz) so as not to significantly disturb the current distribution at

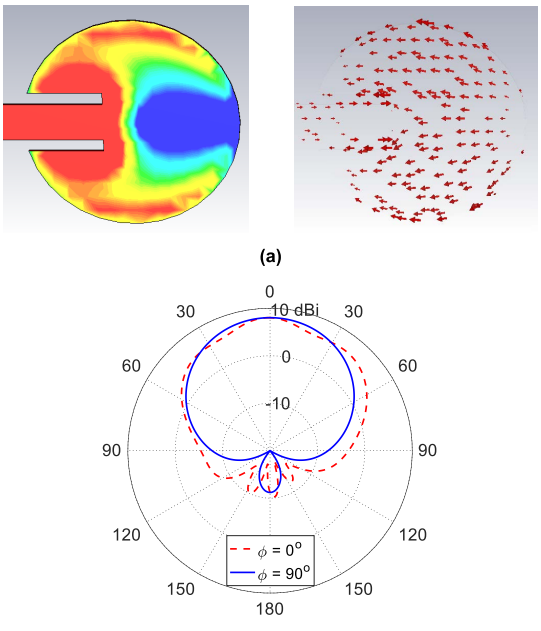

FIGURE 4. (a) Distribution of the magnitude and directions of the surface current at 28 GHz, and (b) The corresponding gain pattern, for a circular patch antenna with inset feed.

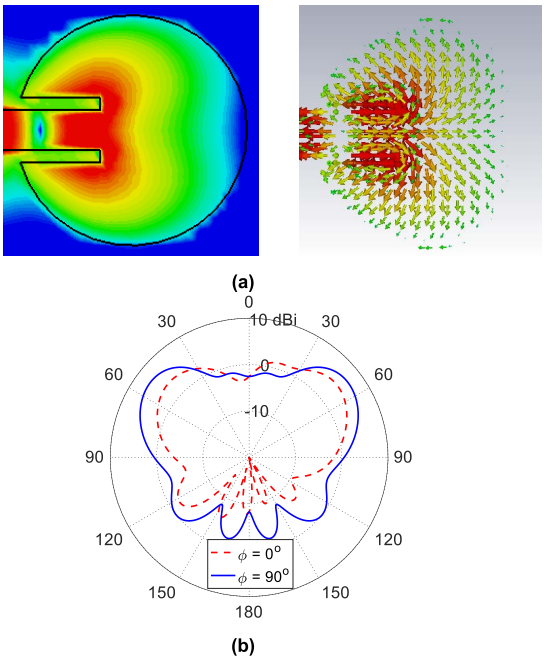

FIGURE 5. (a) Distribution of the magnitude and directions of the surface current at 38 GHz, and (b) The corresponding gain pattern, for a circular patch antenna with inset feed.

this resonance. The cuts made in the patch aim to modify the distribution of the surface current at 38 GHz so as to increase the antenna gain in the direction $\theta = 0°$. The return loss, $|S_{11}|$, over a wide frequency band is shown in Fig. 6. It is clear in the figure that the modified patch has matched impedance at 36.5 GHz which needs to be shifted to the desired frequency of operation at 38 GHz.

Unfortunately, the geometrical modification leads to shift the first resonance frequency to about 27 GHz. Furthermore,

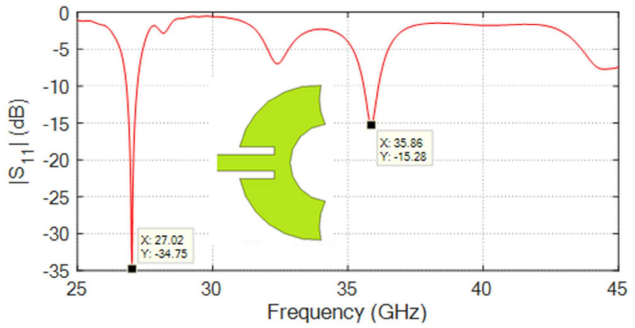

FIGURE 6. The reflection coefficient, $|S_{11}|$ with frequency for the modified circular patch antenna.

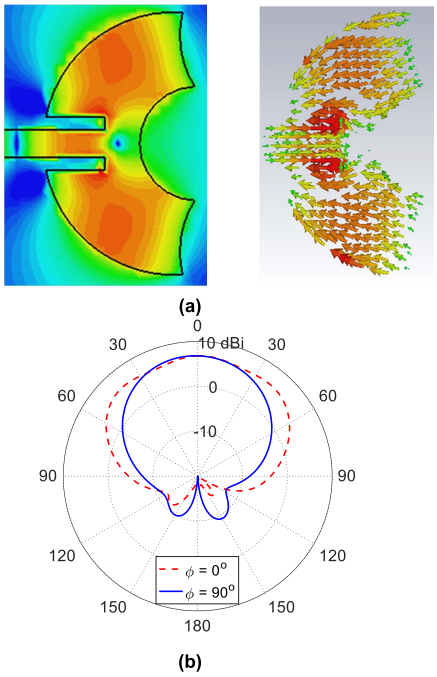

FIGURE 7. (a) Distribution of the magnitude and directions of the surface current at 27.02 GHz, and (b) The corresponding Gain pattern.

the modification of the patch geometry leads to some widening of the radiation pattern at this resonance and consequently, to a slight reduction of the gain in the forward direction to be about 6.7 dBi. This can be attributed to reducing the area of the active region of the patch due to the geometry modification. The current distribution over the surface and the corresponding gain pattern at 27.02 and 35.86 GHz are shown in Fig. 7 and 8, respectively.

It may be useful to compare the surface distribution presented in Fig. 8a to that presented in Fig. 5a. It is clear that the unidirectional x-oriented component of the surface current at 38 GHz is increased relative to the y-oriented component which has opposite directions on the upper and lower half of the modified patch. This improvement of the surface current leads to narrowing the beam and increasing the gain in the forward direction at 38 GHz to be about 2.9 dBi, which is shown by comparison between Figure 8b and 5b. It is worth noting from Figure 7b that the radiation pattern at 28 GHz is not much affected by the modifications performed to the geometry of the patch.

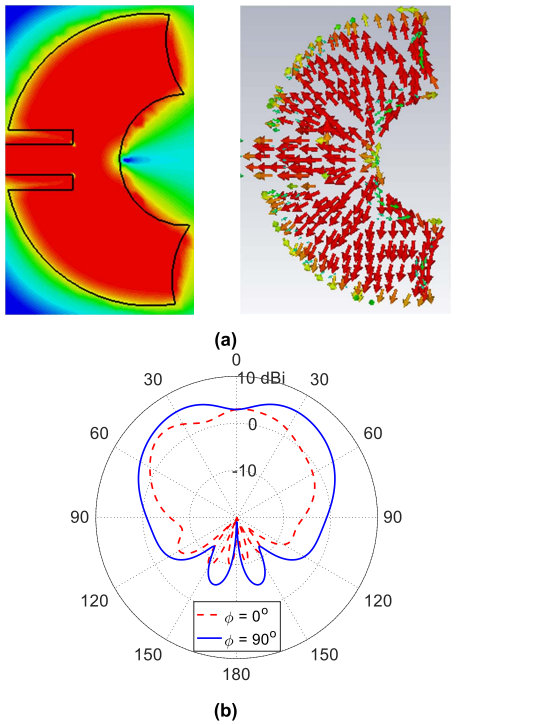

FIGURE 8. (a) Distribution of the magnitude and directions of the surface current at 35.86 GHz, and (b) The corresponding Gain pattern.

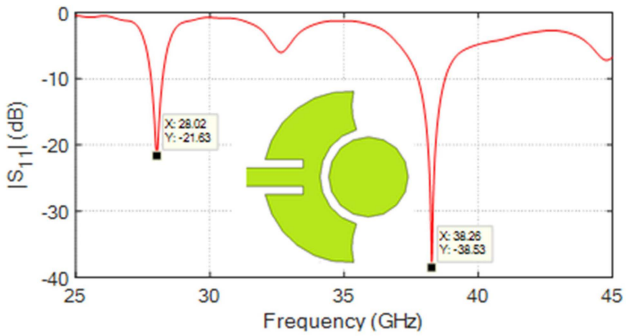

FIGURE 9. Reflection coefficient, $|S_{11}|$, with frequency for the modified circular patch antenna with the parasitic element.

3) DESIGN STAGE 3: ADDING PARASITIC ELEMENT TO THE MODIFIED CIRCULAR PATCH

Modifications of the patch geometry are still required to get the resonance frequencies at 28 and 38 GHz and to increase the gain in the forward direction at 38 GHz. This can be achieved by adding a secondary patch of circular shape to the main patch through capacitive coupling as shown Fig. 9. The return loss, $|S_{11}|$, is shown in the same figure. It is shown that the resonance frequencies are at 28.02 and 38.26 GHz which are much closer to the required frequencies of operation.

The surface current distribution at 28.02 GHz and the corresponding gain pattern are presented in Fig.10. It is clear that the geometrical modifications performed so far keeps the shape of the gain pattern at 28 GHz acceptable for the intended applications commonly required in 5G mobile communications. On the other hand, the current distribution over the patch surface and the resulting gain pattern at 38.26 GHz

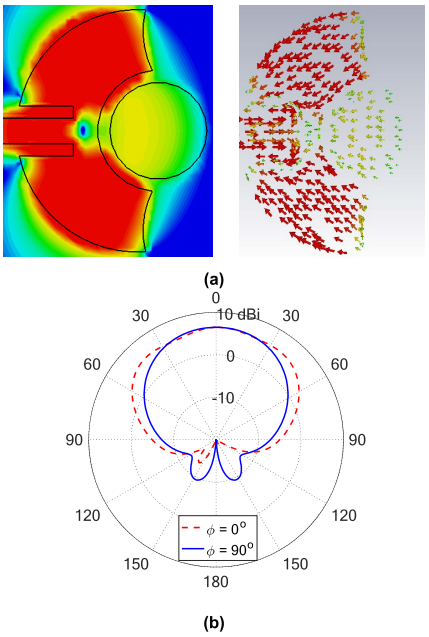

FIGURE 10. (a) Distribution of the magnitude and directions of the surface current at 28.02 GHz, (b) The corresponding Gain pattern.

are presented in Fig. 11. The radiation pattern shows low gain of about -0.76 dBi in the direction $\theta = 0°$. In view of the surface current distribution at 38 GHz shown in Fig. 11a, the reduction of the gain due to the last geometrical modification can be attributed to the current generated on the secondary patch having opposite direction to the current on the primary patch, which causes the gain to be reduced in the direction $\theta = 0°$.

4) DESIGN STAGE 4: MODIFYING THE SHAPE OF THE PARASITIC ELEMENT

According to the above discussion and in order to reduce the current of the opposite direction generated on the secondary patch, it is suggested to laterally increase the area of the parasitic patch so as to act as a reflector as shown in Fig. 12. The lower and upper resonances are located exactly at the required locations (28 and 38 GHz). A defect in the ground is added to widen the impedance bandwidth. The current distributions over the patch surface and the radiation patterns at 28 and 38 GHz are presented in Fig. 13 and 14, respectively. As expected, the current on the parasitic patch is almost diminished at 38 GHz leading to increase the gain in the direction $\theta = 0°$ to about 5.2 dBi as shown in Fig. 14b. The final design parameters are listed in Table 1.

The radiation efficiency of the proposed antenna is 87.5% and 91.3% at 28 and 38 GHz, respectively. The antenna is linearly polarized with cross polarization ratio of about -60 and -75 dB at 28 and 38 GHz.

B. EFFECT OF THE SEPARATION DISTANCE OF THE CAPACITIVE PATCH

The distance between the capacitive patch and the antenna affects the impedance matching. This effect is depicted in Fig. 15 for different coupling distances d. The rest of the dimensions are as listed in Table 1. It is clear from the figure that the minimum of the impedance matching locations change with the coupling distance as the added parasitic element acts as a capacitive load to the primary patch.

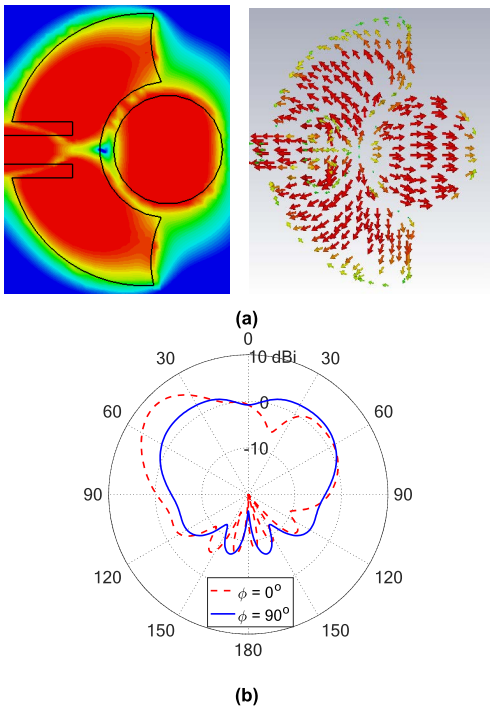

FIGURE 11. (a) Distribution of the magnitude and directions of the surface current at 38.26 GHz, (b) The corresponding Gain pattern.

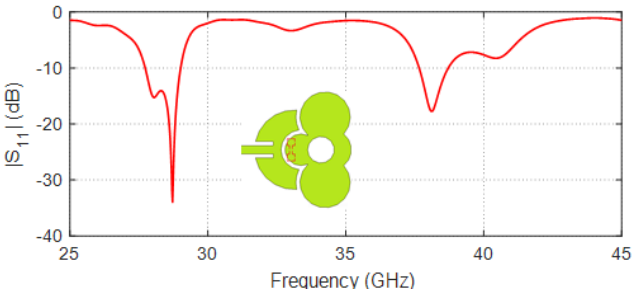

FIGURE 12. The return loss, $|S_{11}|$, with frequency over a wide band for the final design of the proposed patch antenna indicated.

TABLE 1. Final dimensions (mm) of the proposed composite patch antenna.

L_1	0.5	W_o	0.633
L_2	1.5	R_1	1.9
L_3	0.8	R_2	1.5
L_g	2.47	R_g	1.0
L_i	1.4	R_{c1}	1.2
L_o	13.4	R_{c2}	1.5
W_i	0.3	R_p	3.0

C. EFFECT OF THE HUMAN SKIN AND THE MOBILE CHASSIS ON THE ANTENNA PERFORMANCE

Since the proposed antenna design is intended to be placed inside a mobile handset, the effect of the human hand during usage should be studied. The human hand is considered a very

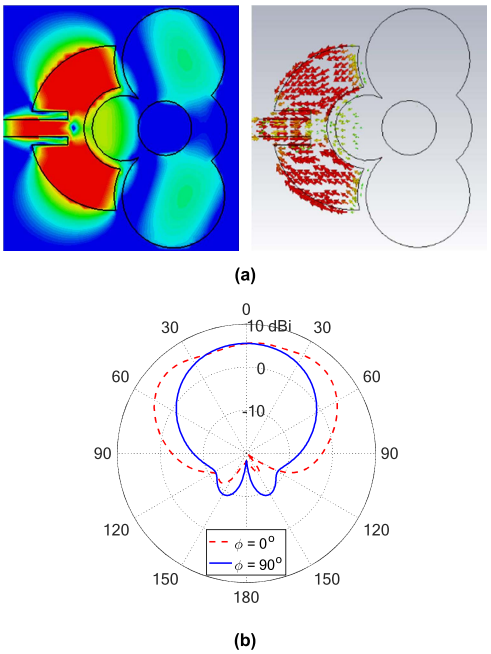

FIGURE 13. (a) Distribution of the magnitude and directions of the surface current of the final patch design at 28 GHz, (b) The corresponding Gain pattern.

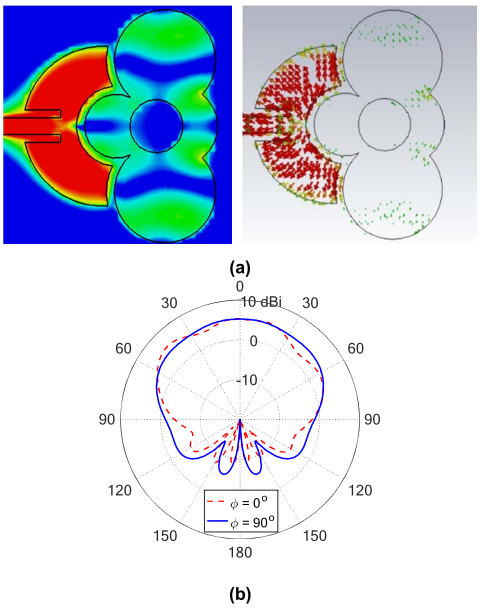

FIGURE 14. (a) Distribution of the magnitude and directions of the surface current of the final patch design at 38 GHz, (b) The corresponding Gain pattern.

huge, electrically large object in the millimetric frequency range. This makes the electromagnetic simulation of the hand effect requires a very large memory which is beyond the capabilities of the computing machine. Also, the penetration depth of the electromagnetic wave is very shallow in the millimetric range. Because of these two reasons, the effect of placing the antenna on a mobile chassis close to the human hand is approximated by placing the antenna over two layers; A 1 mm thick skin layer with electric parameters $\epsilon_r = 10.7$, $\sigma = 7.32\,s/m$ at 28 GHz and $\epsilon_r = 10.05$, $\sigma = 10.25\,s/m$

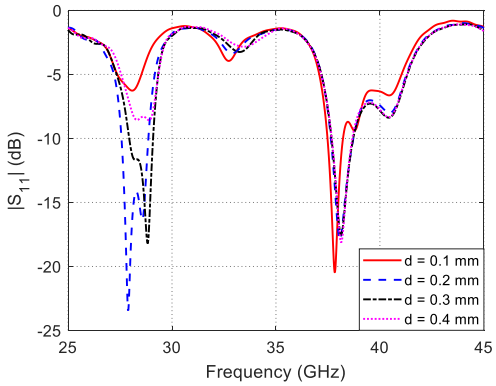

FIGURE 15. Effect of the coupling distance between the parasitic element and the patch antenna.

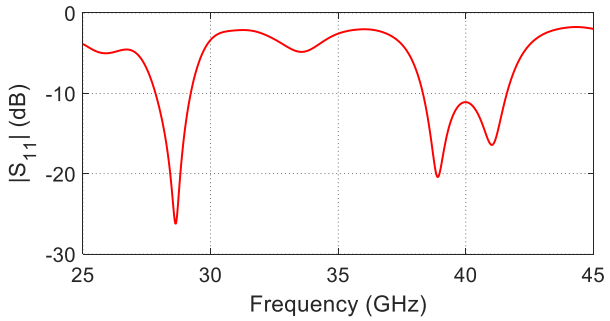

FIGURE 16. Reflection coefficient of the proposed antenna when placed over a simplified model of the mobile chassis and adherent skin.

at 38 GHz [19]; and a 1 mm layer of polypropylene with $\epsilon_r = 2.25$ and $\tan\delta = 0.0001$ [20]. The extension of the layers model beneath the antenna is 40 mm × 40 mm. The resulting reflection coefficient is shown in Figure 16. The radiation patterns of the proposed antenna placed over the simplified model of skin and mobile chassis at 28 and 38 GHz are shown in Figure 17. It is clear from Figure 16 and 17 that the radiation pattern at 28 GHz is much affected than the 38 GHz band by placing the antenna near to a human skin.

D. GAIN AND EFFICIENCY OF THE PROPOSED ANTENNA

The maximum gain of the proposed antenna is calculated over a wide frequency range and plotted in Figure 18. The radiation efficiency is also calculated numerically using the CST taking into consideration the metal and dielectric losses over the frequency band 25-45 GHz. The results are shown in Figure 19. It can be seen that the antenna has 80 and 85% radiation efficiency at the two operating band 28 and 38 GHz, respectively.

E. TWO-PORT MIMO ANTENNA SYSTEM PERFORMANCE

Numerical simulation is performed in this section to assess the performance of the two elements MIMO system. The results of the S-parameters, gain pattern, and diversity parameters are presented and discussed.

1) SIDE-BY-SIDE MIMO ANTENNA SYSTEM CONFIGURATION

The two-port MIMO antenna configuration shown in Fig. 2a is constructed with separation distance $D_y = 23$ mm.

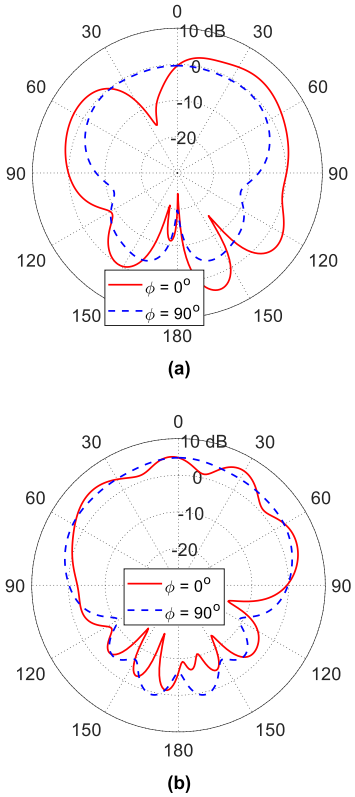

FIGURE 17. Radiation pattern of the proposed antenna placed over a simplified model of the mobile chassis and adherent skin at, (a) 28 GHz, (b) 38 GHz.

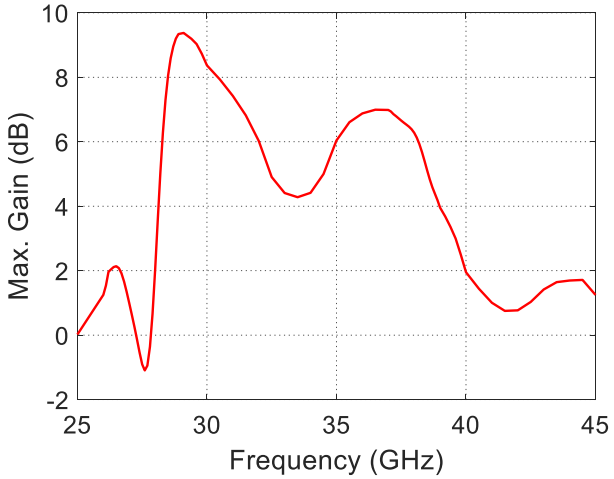

FIGURE 18. Maximum gain versus frequency of the proposed dual-band antenna.

The dimensions of a constructing patch are as listed in Table 1. The total dimension is 13 mm × 23 mm. The reflection and transmission coefficients are shown in Fig. 20. It can be seen that the reflection coefficient is almost the same for all ports. The two antennas are matched at both operating frequency bands. Also the coupling coefficients are very low <-28 dB at both bands. Due to the symmetry in the configuration, the gain pattern of one patch antenna at 28 and 38 GHz is shown in Fig. 21a and 21b, respectively. It can be shown from Fig. 21 that the gain pattern of one patch

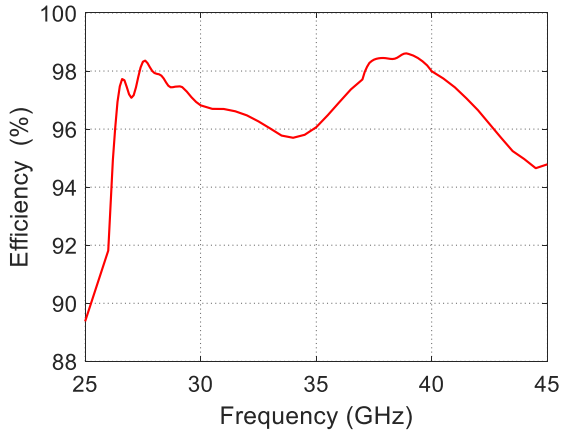

FIGURE 19. Radiation efficiency of the proposed antenna over the frequency band 25-45 GHz.

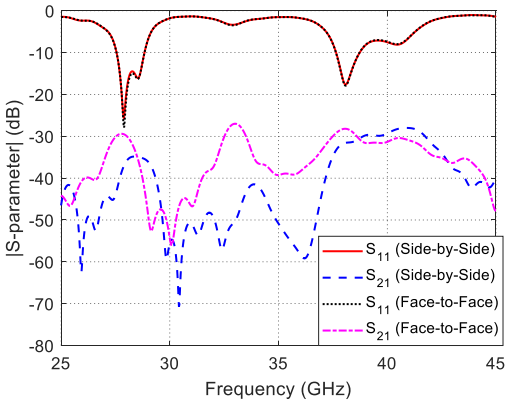

FIGURE 20. Simulated frequency response of the self and mutual coupling coefficients of the side-by-side two-port MIMO antenna system.

antenna in this configuration is almost not affected by the other element. The envelope correlation coefficient and the diversity gain as a measure of the MIMO system performance are calculated and plotted in Fig. 22 showing excellent performance of the proposed side-by-side MIMO antenna system configuration.

2) FONT-TO-FRONT MIMO ANTENNA SYSTEM CONFIGURATION

The two-port MIMO antenna configuration shown in Fig. 2b is constructed with $D_x = 13$ mm. Fig. 20 shows the reflection and the coupling coefficients of the front-to front MIMO antenna system configuration. It is clear that the two antennas have good impedance matching at 28 and38 GHz. The gain pattern of one patch antenna at 28 and 38 GHz is shown in Fig. 23a and 23b, respectively. It can be shown from Fig. 23 that the gain pattern of one patch antenna in this configuration is almost not affected by the other element. The ECC and DG are evaluated and plotted in Fig. 24 showing excellent performance of the proposed MIMO antenna system configuration.

F. FABRICATION AND PRACTICAL MEASUREMENTS

A prototype for the proposed antenna is fabricated for the purpose of assessment of the patch performance and shown

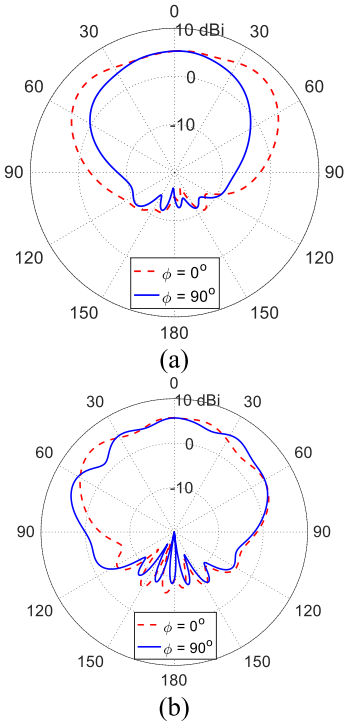

FIGURE 21. Gain patterns of the proposed patch antenna for the 2-port MIMO antenna system in the side-by-side configuration at (a) 28 GHz, (b) 38 GHz.

in Figure 25a. The fabrication process is performed through photolithography.

1) MEASUREMENTS OF THE REFLECTION COEFFICIENT

The vector network analyzer (VNA) Rhode and Schwartz model ZVA67 is used for measuring the frequency response of the reflection coefficient S_{11}. In order to connect the fabricated prototype to the VNA, an end-launch connector 2.4 mm from Southwest Microwave Inc. is used for this purpose. The connection and the experimental setup are shown in Figure 25b. A calibration process is performed at the VNA ports in the frequency range 25-45 GHz before measuring the reflection coefficient.

The frequency response of the reflection coefficient $|S_{11}|$ is presented in Figure 26 as measured by the ZVA67. The simulation and measurement results for the frequency dependencies of $|S_{11}|$ are compared and presented in the same figure showing good agreement. The upper and lower measured operation frequencies are centered at 27.9 GHz and 38 GHz, respectively. The impedance matching bandwidths (for $|S_{11}| < -10$ dB) obtained through measurements are about 3% at 28 GHz and about 3.2% at 38 GHz. It is worth noting that the impedance matching bandwidth obtained from the simulated $|S_{11}|$ is 5% and 3.5% at 28 GHz and 38 GHz, respectively.

2) MEASUREMENTS OF THE RADIATION PATTERNS

The radiation patterns and the maximum gain of the proposed antenna are measured at 28 and 38 GHz. The experimental

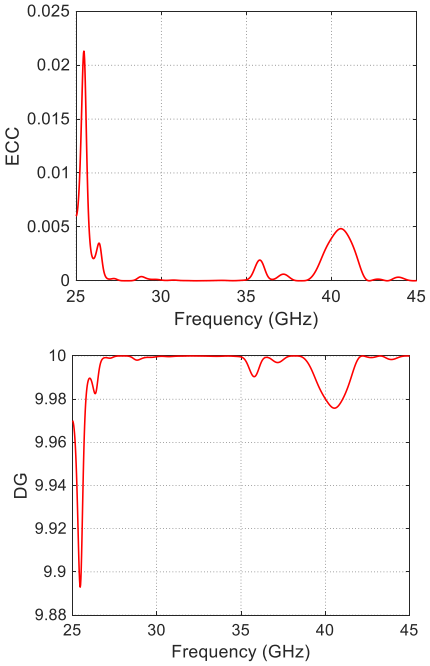

FIGURE 22. Frequency dependence of the ECC and DG of the side-by-side MIMO antenna proposed in the present work.

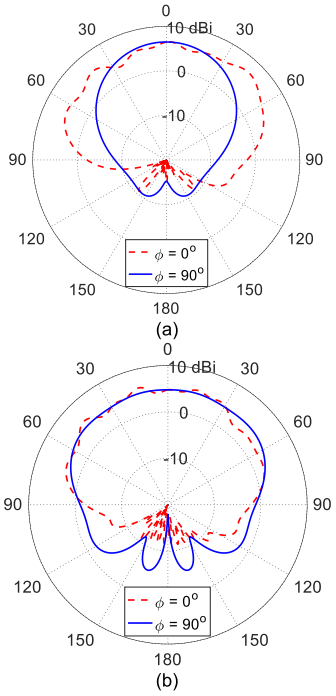

FIGURE 23. Gain patterns of the proposed patch antenna for the 2-port MIMO antenna system in the front-to-front configuration at (a) 28 GHz, (b) 38 GHz.

setup is presented in Figure 27. The VNA Rhode and Schwartz model ZVA67 is set to operate in the two-port measurement mode for the purpose of measuring the transmission coefficient $|S_{21}|$ through the antenna under test (port 1) and the reference-gain antenna (port 2). LB-018400 is the reference gain linearly-polarized horn employed in the measurements. The separation between the two antennas is 30 cm.

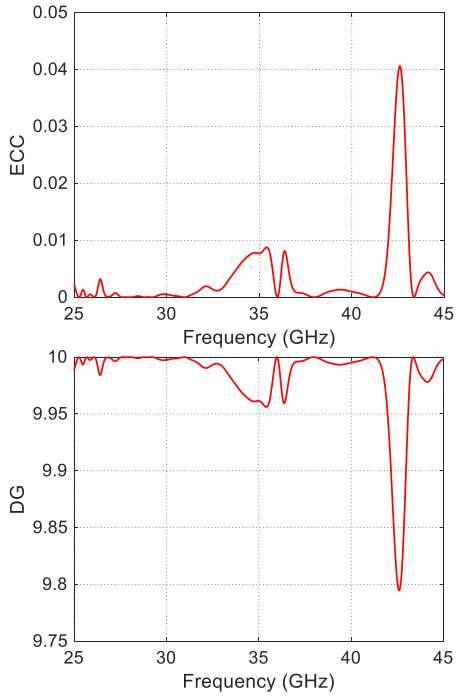

FIGURE 24. Frequency dependence of the ECC and DG of the front-to-front MIMO antenna proposed in the present work.

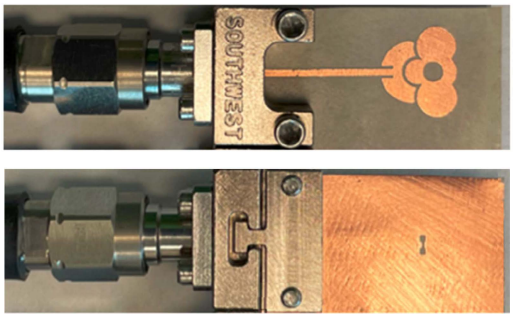

(a)

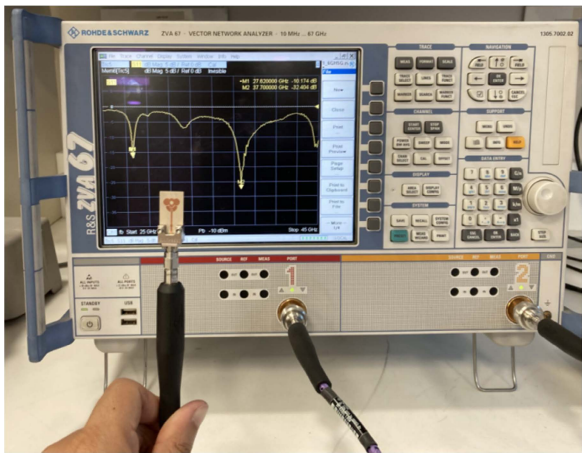

(b)

FIGURE 25. Measuring the reflection coefficient $|S_{11}|$, (a) fabricated prototype with the mounted 2.4 mm end-launch connector, (b) experimental setup with the antenna connected to the VNA ZVA67.

The radiation patterns in the elevation planes $\phi = 0°$ and $\phi = 90°$ corresponding to the E-plane and H-plane,

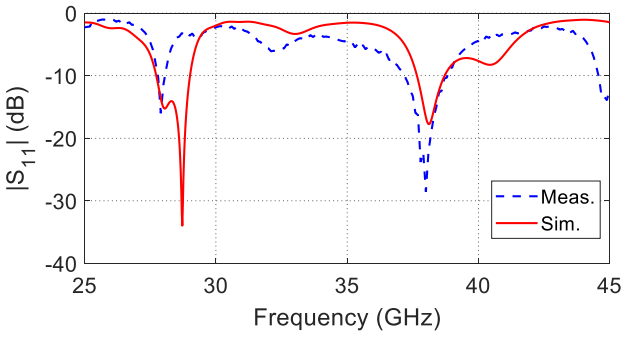

FIGURE 26. Measured frequency responses of the reflection coefficient $|S_{11}|$ of the proposed antenna.

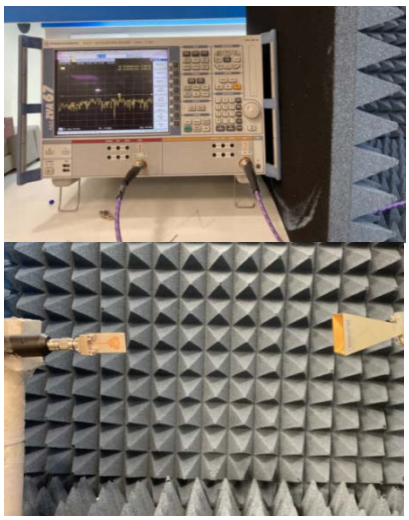

FIGURE 27. Experimental setup for measuring the radiation pattern and gain of the proposed dual-band patch antenna.

respectively, are measured for the proposed patch antenna, and presented in Figure 28 and Figure 29 at the frequencies 28 GHz and 38 GHz, respectively. It is clear from the two figures that the measured and simulated radiation patterns are close to each other and show good agreement. The measured maximum gain for the proposed patch antenna are 6.2 dBi and 5.3 dBi at 28 GHz and 38 GHz, respectively, which are close to the simulated values (6.6 dBi and 5.86 dBi at 28 GHz and 38 GHz, respectively).

3) MEASUREMENT OF THE PERFORMANCE OF THE PROPOSED MIMO SYSTEM CONFIGURATIONS

In this section, the proposed dual-band antenna is employed to construct a two-port MIMO antenna system for a mobile phone handset in the two different configurations shown in Figure 2. The fabricated prototypes for the side-by-side and front-to-front MIMO system configurations are shown in Figure 30a, and 30b, respectively. The frequency response of the reflection and transmission coefficients for each configuration is measured using the VNA Rhode & Schwartz model ZVA67 and plotted in Figure 31. It is evident that the MIMO antenna system exhibits good impedance matching at both of the operating frequencies 28 and 38GHz. The measured

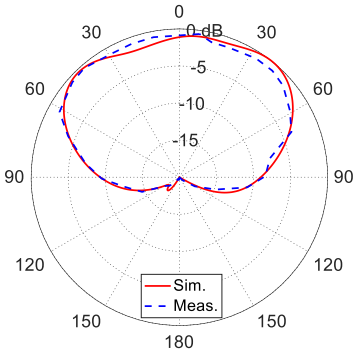

(a) E-plane ($\phi = 0°$)

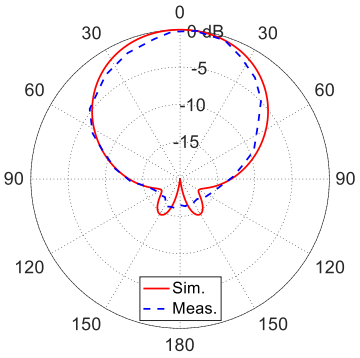

(b) H-plane ($\phi = 90°$)

FIGURE 28. Measured radiation and simulated radiation patterns of the proposed dual-band microstrip patch antenna at 28 GHz in the two principle planes.

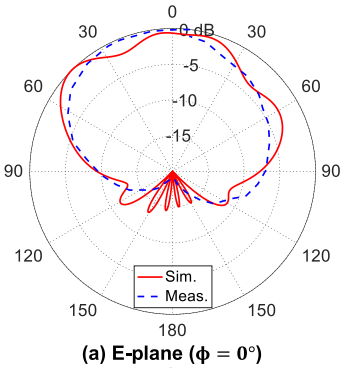

(a) E-plane ($\phi = 0°$)

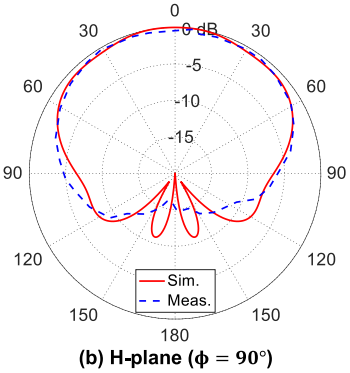

(b) H-plane ($\phi = 90°$)

FIGURE 29. Measured radiation and simulated radiation patterns of the proposed dual-band microstrip patch antenna at 38 GHz in the two principle planes.

mutual coupling coefficients has very low value <-20 dB over the entire frequency range for both configurations.

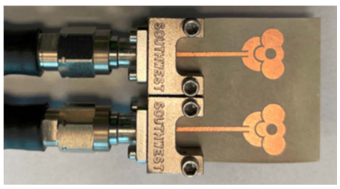

(a)

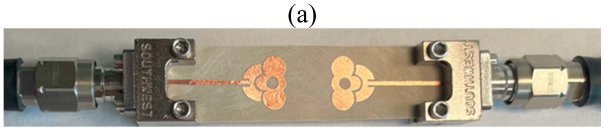

(b)

FIGURE 30. Fabricated prototype for the two-port, (a) side-by-side, (b) front-to-front, MIMO antenna system configurations.

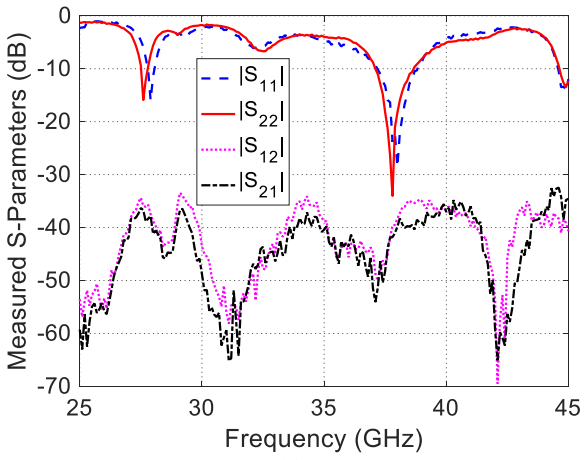

(a)

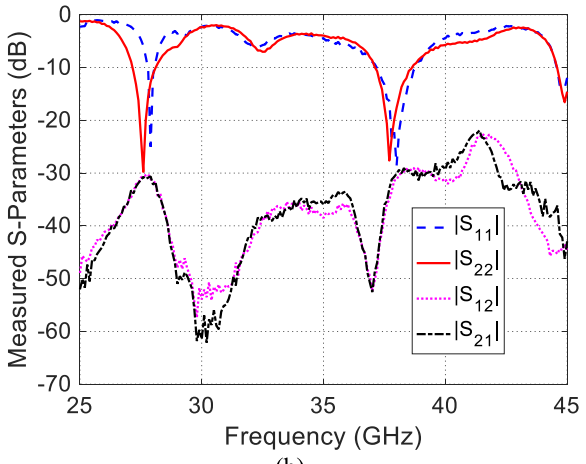

(b)

FIGURE 31. Measured frequency response of the self and mutual coupling coefficient of the proposed two-port (a) side-by-side, (b) front-to-front, MIMO antenna system.

G. COMPARISON WITH SIMILAR PUBLISHED WORK

The proposed antenna is compared to other published mm-wave antennas intended for future 5G applications. The patch antenna of this work combines the compactness in size, multi-band operation, and ease of integration. All these traits are required for the future 5G portable devices. Table 2 compares the proposed antenna with similar antenna found in literature from the point of view of the frequency of operation, size, and impedance matching.

TABLE 2. Comparison with published work.

Reference	Frequency of Operation (GHz)	Size (mm^3)	Impedance Matching (dB)
[17]	28/38/48	34.8 × 34.8 × 0.508	-20/-25/-30
[15]	28/38	11 × 9 × 0.135	-35/-32
[21]	28/38	14 × 12 × 0.38	-22/-16
[2]	28/38	21.6 × 20 × 0.25	-31/-36
Present Work	28/38	7.5 × 8.8 × 0.25	-24/-20

V. CONCLUSION

In this work, a compact dual-frequency band (28/38 GHz) microstrip patch antenna design for 5G mobile handsets is presented. The proposed antenna is composed of two patches, primary feeding patch and secondary parasitic patch. The development stages of the antenna design are presented showing the complicated radiation mechanisms involved. A prototype is fabricated and measured. Numerical and experimental results are compared showing good performance regarding reflection coefficient, bandwidth, radiation patterns, and gain. The impedance matching bandwidths are about 5% at 28 GHz and about 3.5% at 38 GHz. The minimum value of the reflection coefficient for 28 GHz band is −34.5 dB and is −27.3 for 38 GHz. The measured radiation patterns are have a peak gain of 6.6 dBi and 5.86 dBi at 28 GHz and 38 GHz, respectively. For both bands, the radiation patterns are omnidirectional, which makes the proposed patch antenna an excellent candidate for 5G MIMO systems.

REFERENCES

[1] S. Muhammad, A. S. Yaro, I. Yau, and A. T. Salawudeen, "Design of 5G mobile millimeter wave antenna," *ATBU J. Sci., Technol. Educ.*, vol. 7, no. 2, pp. 178–184, 2019.

[2] M. Abirami, "A review of patch antenna design for 5G," in *Proc. IEEE Int. Conf. Electr., Instrum. Commun. Eng. (ICEICE)*, Apr. 2017, pp. 1–3.

[3] P. A. Dzagbletey and Y. B. Jung, "Stacked microstrip linear array for millimeter-wave 5G baseband communication," *IEEE Antennas Wireless Propag. Lett.*, vol. 17, no. 5, pp. 780–783, May 2018.

[4] A. Rachakonda, P. Bang, and J. Mudiganti, "A compact dual band MIMO PIFA for 5G applications," *IOP Conf. Ser., Mater. Sci. Eng.*, vol. 263, Nov. 2017, Art. no. 052034.

[5] O. M. Haraz, "Broadband and 28/38-GHz dual-band printed monopole/elliptical slot ring antennas for the future 5G cellular communications," *J. Infr., Millim., THz Waves*, vol. 37, no. 4, pp. 308–317, Apr. 2016.

[6] G. Ancansa, V. Bobrovsa, A. Ancansb, and D. Kalibatiene, "Spectrum considerations for 5G mobile communication systems," *Proc. Comput. Sci.*, vol. 104, pp. 509–516, Sep. 2016.

[7] J. Saini and S. K. Agarwal, "Design a single band microstrip patch antenna at 60 GHz millimeter wave for 5G application," in *Proc. Int. Conf. Comput., Commun. Electron.*, 2017, pp. 227–230.

[8] J. Restrepo, "Spectrum allocation for 5G international framework," in *Proc. Inf. Commun. Technol. Eur. CIS*, Odessa, Ukraine, 2019, pp. 30–31.

[9] A. E. Farahat and K. F. A. Hussein, "28/38 GHz dual-band Yagi-Uda antenna with corrugated radiator and enhanced reflectors for 5G MIMO antenna systems," *Prog. Electromagn. Res. C*, vol. 101, pp. 159–172, 2020.

[10] J. Kornprobst, K. Wang, G. Hamberger, and T. F. Eibert, "A mm-wave patch antenna with broad bandwidth and a wide angular range," *IEEE Trans. Antennas Propag.*, vol. 65, no. 8, pp. 4293–4298, Aug. 2017.

[11] M. Mantash, A. Kesavan, and T. A. Denidni, "Beam-tilting endfire antenna using a single-layer FSS for 5G communication networks," *IEEE Antennas Wireless Propag. Lett.*, vol. 17, pp. 29–33, 2018.

[12] S. Li, T. Chi, Y. Wang, and H. Wang, "A millimeter-wave dual-feed square loop antenna for 5G communications," *IEEE Trans. Antennas Propag.*, vol. 65, no. 12, pp. 6317–6328, Dec. 2017.

[13] J. S. Park, J.-B. Ko, H.-K. Kwon, B.-S. Kang, B. Park, and D. Kim, "A tilted combined beam antenna for 5G communications using a 28-GHz band," *IEEE Antennas Wireless Propog. Lett.*, vol. 15, pp. 1685–1688, 2016.

[14] H. Aliakbari, A. Abdipour, R. Mirzavand, A. Costanzo, and P. Mousavi, "A single feed dual-band circularly polarized millimeter-wave antenna for 5G communication," in *Proc. 10th Eur. Conf. Antennas Propag. (EuCAP)*, Apr. 2016, pp. 1–5.

[15] S. F. Jilani and A. Alomainy, "An inkjet-printed MMW frequency-reconfigurable antenna on a flexible PET substrate for 5G wireless systems," in *Proc. Loughborough Antennas Propag. Conf. (LAPC)*, 2017, pp. 1–3.

[16] Q. Wu, J. Yin, C. Yu, H. Wang, and W. Hong, "Low-profile millimeter-wave SIW cavity-backed dual-band circularly polarized antenna," *IEEE Trans. Antennas Propag.*, vol. 65, no. 12, pp. 7310–7315, Dec. 2017.

[17] K. R. Mahmoud and A. M. Montaser, "Performance of tri-band multi-polarized array antenna for 5G mobile base station adopting polarization and directivity control," *IEEE Access*, vol. 6, pp. 8682–8694, 2018.

[18] Z. Wani, M. P. Abegaonkar, and S. K. Koul, "A 28-GHz antenna for 5G MIMO applications," *Prog. Electromagn. Res. Lett.*, vol. 78, pp. 73–79, 2018.

[19] H. Zhao, Q. Wang, and K. Shi, "Analysis on human blockage path loss and shadow fading in millimeter-wave band," *Int. J. Antennas Propag.*, vol. 2017, pp. 1–6, Dec. 2017.

[20] J. Krupka, "Measurements of the complex permittivity of low loss polymers at frequency range from 5 GHz to 50 GHz," *IEEE Microw. Wireless Compon. Lett.*, vol. 26, no. 6, pp. 464–466, Jun. 2016.

[21] M. N. Hasan, S. Bashir, and S. Chu, "Dual band omnidirectional millimeter wave antenna for 5G communications," *J. Electromagn. Waves Appl.*, vol. 33, no. 12, pp. 1581–1590, Aug. 2019.

ASMAA E. FARAHAT received the B.Sc. and M.Sc. degrees from the Department of Biomedical Engineering, Faculty of Engineering, Cairo University, in 2002 and 2006, respectively, and the Ph.D. degree from Ain Shams University, in 2012. She is currently an Associate Professor with the Department of Microwave Engineering, Electronics Research Institute. She has work experience in scientific research for about 17 years. She has published more than 30 papers in international, regional, and local scientific journals and conferences. She has worked as a secondary investigator for three research projects. Her research interests include in the areas of antennas, electromagnetic wave propagation, risk assessment of human exposure to microwave radiation, remote sensing systems, and radar systems.

KHALID F. A. HUSSEIN received the B.Sc., M.Sc., and Ph.D. degrees from the Department of Electronics and Electrical Communications, Faculty of Engineering, Cairo University, in 1990, 1995, and 2001, respectively. He has served as the Head for the Microwave Engineering Department, Electronics Research Institute, for up to four years, where he is currently a Professor. He has worked as a principal investigator for four research projects and the head of the research group in four other research projects. He designed and implemented several satellite antennas between prototypes and finished products. He has provided scientific consultations and conducted field measurements related to the design and distribution of mobile communication base station antennas for good signal coverage in behalf of many Egyptian and international companies. He has work experience in scientific research for more than 29 years. He has teaching experience in engineering colleges in many universities for more than 20 years. He has supervised more than 70 doctoral and master's theses. He has published more than 100 papers in international, regional, and local scientific journals and conferences. His research interests include in the areas of antennas, electromagnetic wave propagation, risk assessment of human exposure to microwave radiation, optical communications, photonics, quantum computing, radar systems, particularly ground penetrating radar (GPR), synthetic aperture radar (SAR), and remote sensing systems. He has been a member of the Egyptian Space Program (currently the Egyptian Space Agency) for more than eight years.